Skin-Core Structure–Fatigue Behavior Relationships for Injection-Molded Parts of Polypropylene. I. Influence of Molecular Weight and Injection Conditions on the Morphology

JEAN-PIERRE TROTIGNON and JACQUES VERDU, *Ecole Nationale Supérieure D'Arts et Métiers, Département Materiaux, 151 Boulevard de l'Hôpital, 75640 Paris Cedex 13, France*

Synopsis

The skin-core structure of various injection-molded samples of PP differing by molecular weight and the injection conditions—essentially injection rate and holding pressure—has been studied by microscopy, DSC, WAXS, and IR dichroïsm on microtome sections. The depth distributions of the degree of crystallinity, macromolecular orientation, and beta phase fraction reveal a complex stratification of the morphology. The importance of the holding pressure and its delay of application after the mold filling are underlined.

INTRODUCTION

In the case of injection molding, the melt orientation and cooling rate can differ noticeably from one point to another of the mold cavity. It is therefore not surprising to find pronounced morphological heterogeneïties in injection-molded parts of semicrystalline polymers, especially polypropylene (PP).[1-8] The best known aspect of these heterogeneïties is the so called skin-core structure in which three, more or less distinguishable, layers can be observed.

The outer one (the "skin") is essentially characterized by a relatively high amorphous content due to its quenching by conduction with the metallic walls of the mold. In the inner one (the "core"), the low cooling rate, due to the low thermal conductivity of the polymer, allows a complete relaxation of orientation and, at least in the case of PP, an isotropic spherulitic growth. The skin and core zones are separated by a "shear zone" whose structure, as revealed by microscopy, is characterized by the presence of row nucleated spherulites,[1] which are typical of a crystallization from an oriented melt.[9]

This subdivision in three zones is generally based on microscopic observations.[1,6] It seemed to us interesting to apply other well-known methods of investigation—DSC, IR dichroïsm, and WAXS—in order to quantify the observed morphological contrasts, in the case of PP. Moreover, we shall try to study the eventual relations between these heterogeneïties and some important technical parameters such as the molecular weight of the polymer or the dynamics of the holding pressure set up in the mold cavity. The repercussions of these phenomena on the fatigue behavior of injection-molded parts will be analyzed in the second part of this paper.

Journal of Applied Polymer Science, Vol. 34, 1–18 (1987)

CCC 0021-8995/87/010001-18$04.00

TABLE I
Characteristics of Polymers under Study[a]

Polypropylene designation	PP 5	PP 12	PP 40
MFI 2	5	12	40
Melting temp (°C)	166	166	165
$\overline{M}_n$	72,000	53,000	53,000
$\overline{M}_w$	231,000	220,000	158,000
Tensile yield stress (MPa)	35	36	35
Flexural modulus (MPa)	1600	1500	1700
Trade name	3050 MNI	3120 MNI	3400 MAI

[a]MFI = melt flow index; $\overline{M}_n$ and $\overline{M}_w$ are the number and weight average molecular weights, respectively.

EXPERIMENTAL

Materials

Polypropylenes under study are industrial homopolymers free of nucleating agents and fillers, supplied by Atochem (France). Some of their characteristics, including tensile data, are given in Table I.

Test Specimens

The injection-molded parts are tensile test bars according to NFT 51034 French Standard. Their overall length, calibrated length and thickness are, respectively, 150, 50, and 4 mm. The bars have been arbitrarily divided in sections numbered from one (near the injection gate), to seven (opposite head) (Fig. 1).

Injection Molding

A 250 tons Creusot-Loire Somi screw injection machine was used with two sets of operating parameters: 82 and 83 differing essentially by the injection rate (Fig. 2) and the holding pressure whose variations with time are presented, only for PP/12, in Figure 3. The main injection parameters are listed in Table II.

We shall use a designating code illustrated by the following example: PP/12/82 1G5: PP of melt flow index 12; molded in conditions 82; in a single gate mold cavity (1G), the analysis being made in the fifth section (Fig. 1). The samples were stored in the dark for 6 months at ambient temperature before investigation.

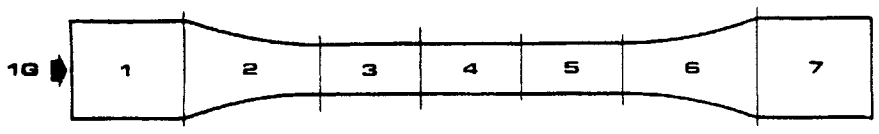

Fig. 1. Analyzed sections in the tensile bar.

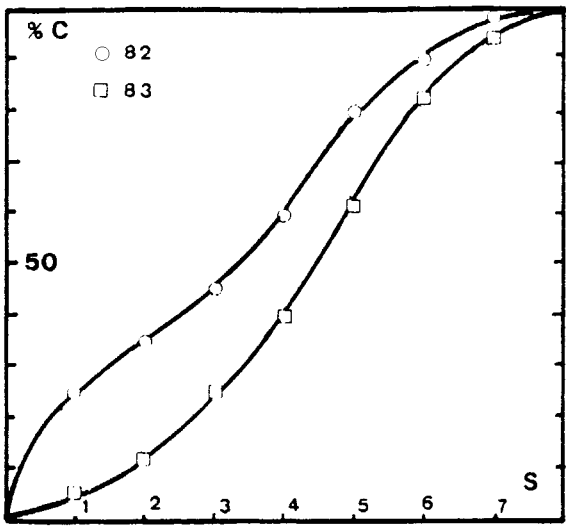

Fig. 2. Screw relative displacement versus time for the two experiments: C = screw displacement; s = steps of regulation

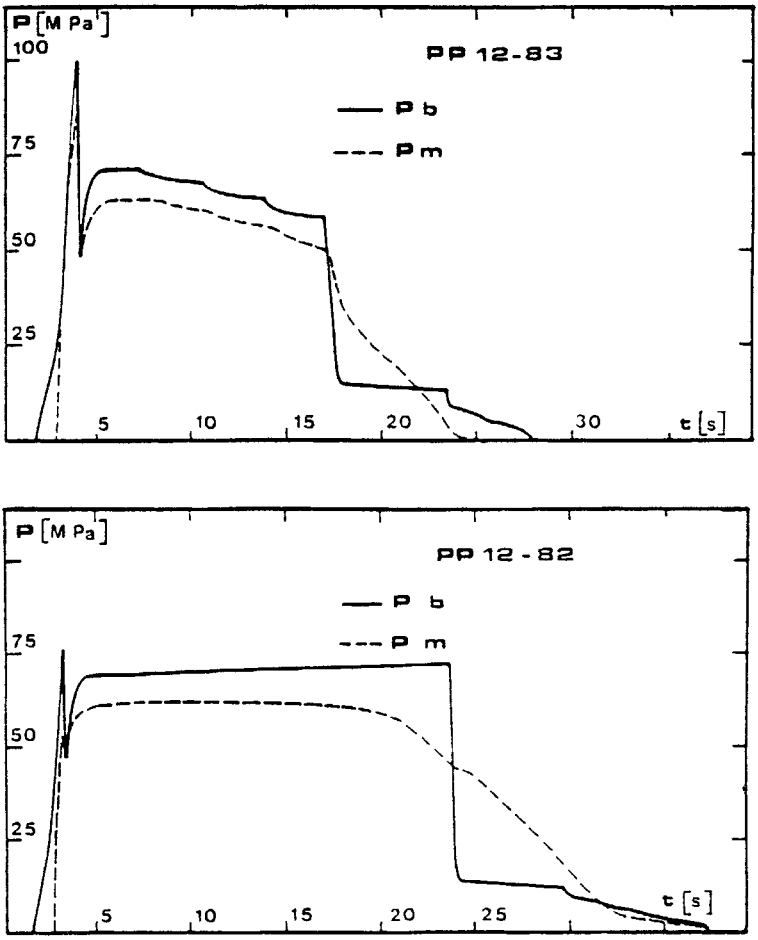

Fig. 3. Pressure variations for the two experiments: P_b = nozzle pressure; P_m = mold pressure.

TABLE II
Injection Parameters

Setting conditions / Injection parameters		82	83
Injection time (s)		2.0	2.3
Injection speed		See fig. 2	
Molding time (s)		20	13
Injection pressure		See fig. 3	
Temperatures (° C)	Feeding zone	150	
	Zone 2	170	
	Zone 3	180	
	Zone 4	200	
	Nozzle	200	
Mold temperature (° C)		38	
Molding time (s)		30	

Analysis

Microtome sections of 5–40 μm thickness (depending on the method of analysis), were cut with a Reichert–Jung microtome equipped with glass or steel blades, at ambient temperature, and then analyzed by:

- DSC using a Perkin-Elmer DSC 2 apparatus, at 20 K min^{-1} scanning rate with 2–5 mg samples. The degree of crystallinity is determined from the melting endotherm, by the usual method.
- WAXS using a CGR σ 2080 diffractometer with a CuK_α anticathode. Two indices A and B were determined as previously described.[10] A is an orientation index: $A = 1$ for a crystallite orientation along the flow direction (longitudinal axis of the tensile bar), and $A = 0$ for any other orientation. B is the Turner-Jones index,[11] characterizing the beta phase. $B = 0$ if no beta phase is found. B = 1 when all the crystalline matter is composed of beta form.
- IR dichroïsm using a Perkin-Elmer 580 spectrophotometer. The crystalline (998 cm^{-1}) and average (1168 cm^{-1}) dichroïc ratios were determined according to Samuels.[12]
- Optical microscopy, using an Olympus BHM microscope for observations in transmission on transveral (T) slices, whereas all the other analysis are made on longitudinal (P) slices (Fig. 4).

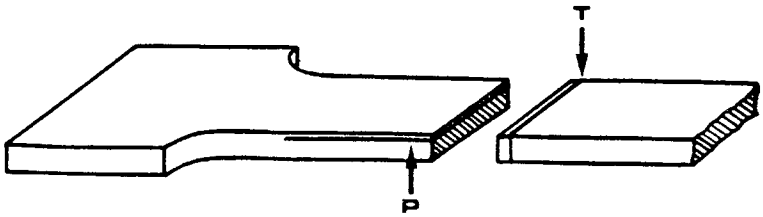

Fig. 4. Microtome cuts.

RESULTS

Our investigations will be focused essentially on section 5 of the sample, because it is the stressed section in our fatigue experiment (Part II of this paper). However, some additional results concerning section 3 of the calibrated section of the tensile bar will be given. More details on the longitudinal phase distributions in these samples have been reported in a previous paper.[10]

Optical Microscopy

Some micrographs of the T slices are shown in Figures 5(a)–(d). It can be clearly seen that the three layers model is too simple, at least for the samples of higher molecular weight (PP/5 and PP/12), to describe the morphology, when four layers are clearly distinguished. Starting from the surface, they can be described as follows:

Zone I (Skin). No visible crystalline structure is observed. The thickness of this layer is about 20 μm.

Zone II. It appears as a bright band of 30–100 μm thickness, characterized by the presence of a fine but visible spherulitic structure.

Zone III. It is a wide dark band (200–300 μm thick), in which no crystalline structure can be distinguished, even at high magnification.

Zone IV (Core). This inner (and thicker) zone contains almost spherical spherulites, whose diameter increases more or less regularly from zone III to the center.

In the case of the sample of lower molecular weight (PP/40), the zones II and III cannot be observed [Fig. 5(d)]. The spherulite diameter is generally smaller than for the samples of higher molecular weight, owing to the increase of the spherulite growth rate due to the low melt viscosity.

DSC

The variations of the degree of crystallinity with the depth are presented in Figures 6(a)–(d). The curves confirm the optical observations: four zones of alternating low and high crystalline ratio can be distinguished, their location and width are well correlated with those of the above-defined zones I–IV. The location of the "secondary crystalline peak" (the "primary" one being in the center of the sample), in zone II, is almost the same for PP/5 and 12/83 molded in the same conditions: 100–140 μm depth; it is noticeably shifted towards the core (230 μm) for PP/40 or PP 12/82.

As expected, the degree of crystallinity in the core decreases when the molecular weight increases.[13]

WAXS

The orientation (A) and beta phase (B) indices are plotted respectively in Figures 7(a)–(d) and 8(a)–(c) for the section 5 of all the samples under study, and in Figures 9 (a)–(c) and 10 (a)–(c) for the section 3 of PP 12/82, PP 12/83 and PP 40/83. These results call the following comments:

- Many workers pointed out that the maximum orientation is located in the skin[1,5,14]; however, the latter was not precisely defined. It is clear, from our results, that the superficial layer (I) of almost 20 μm thickness is less

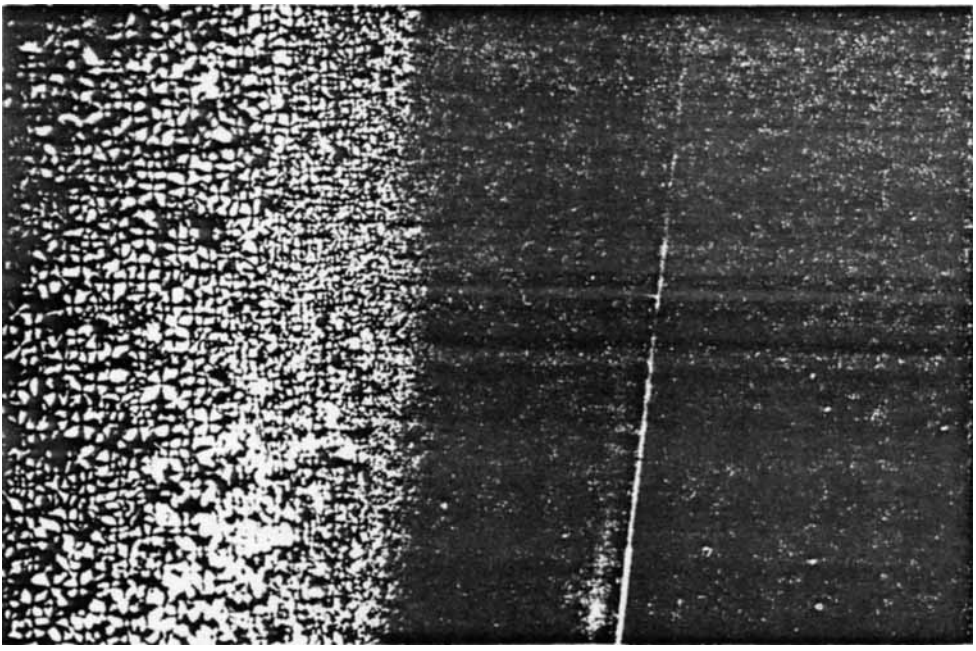

(a)

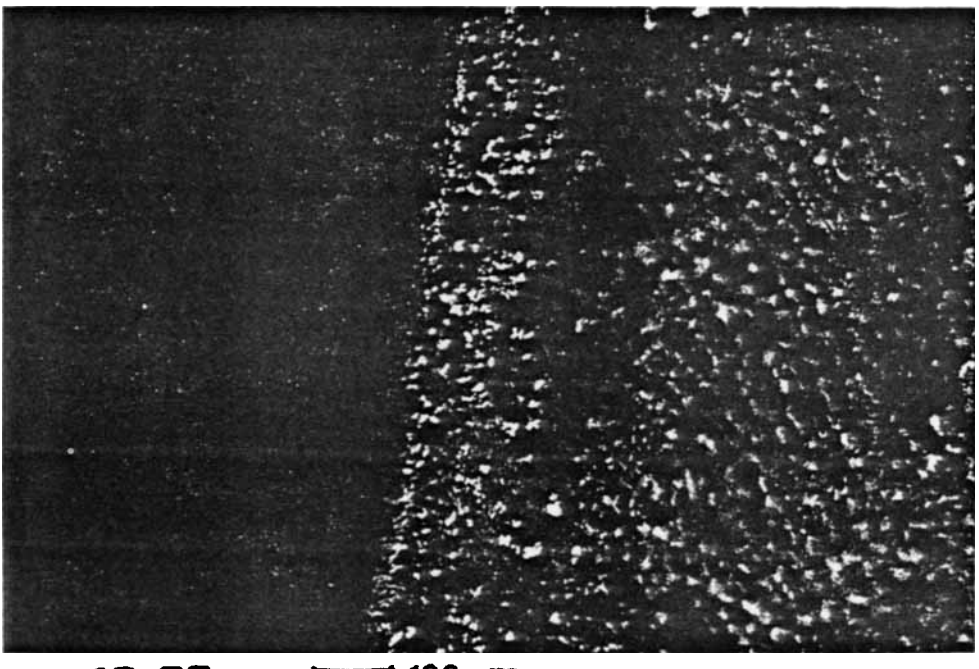

(b)

Fig. 5. Optical micrographs of T slices: (a) PP/5/83 1G5; (b) PP/12/82 1G5; (c) PP/12/83 1G5; (d) PP/40/83 1G5.

(c)

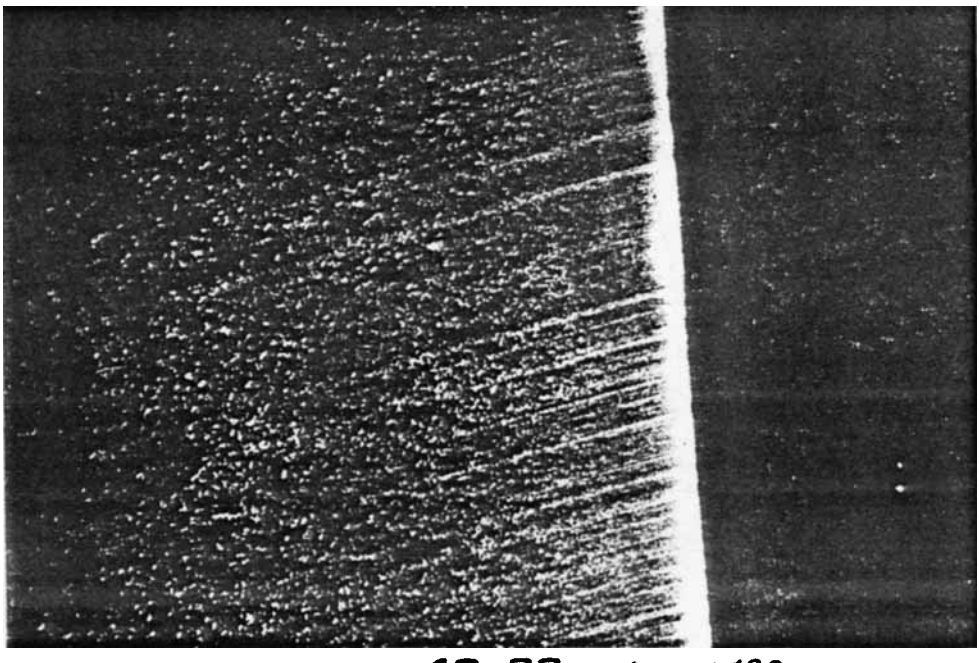

(d)

Fig. 5. (*Continued from the previous page.*)

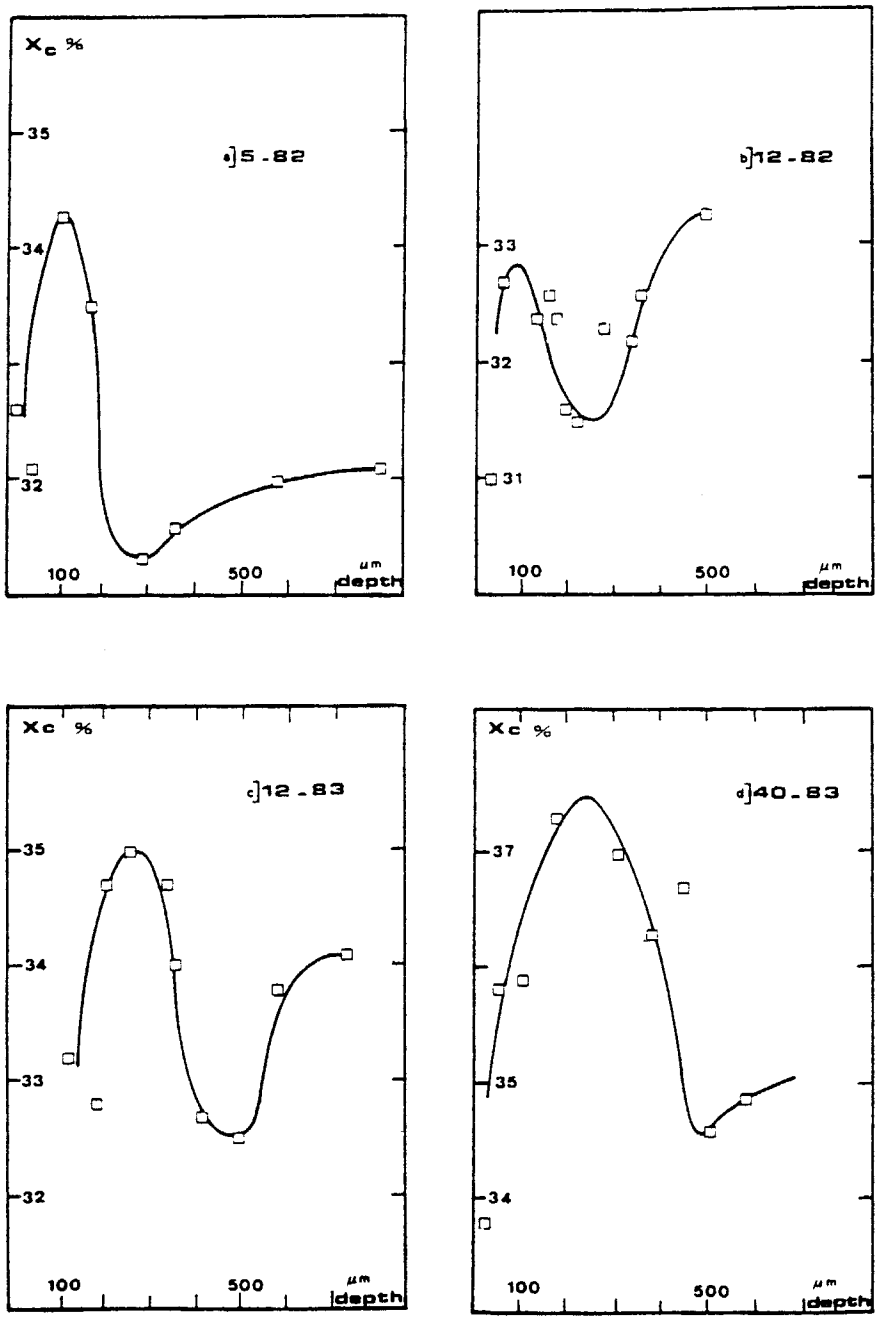

Fig. 6. Depth distribution of X_c from DSC measurements for the 1G5 section: (a) PP/5/82; (b) PP/12/82; (c) PP/12/83; (d) PP/40/83.

oriented than the adjacent one (II). This is consistent with Tadmor's model,[15] which attributes the skin orientation to elongational forces developed at the front of flow, whereas a more efficient subskin orientation process is induced by shear forces.

- It is interesting to note that the orientation factor in zone II is almost unity for PP/5 and PP/12 (except for the section 3 of PP 12/83), and noticeably

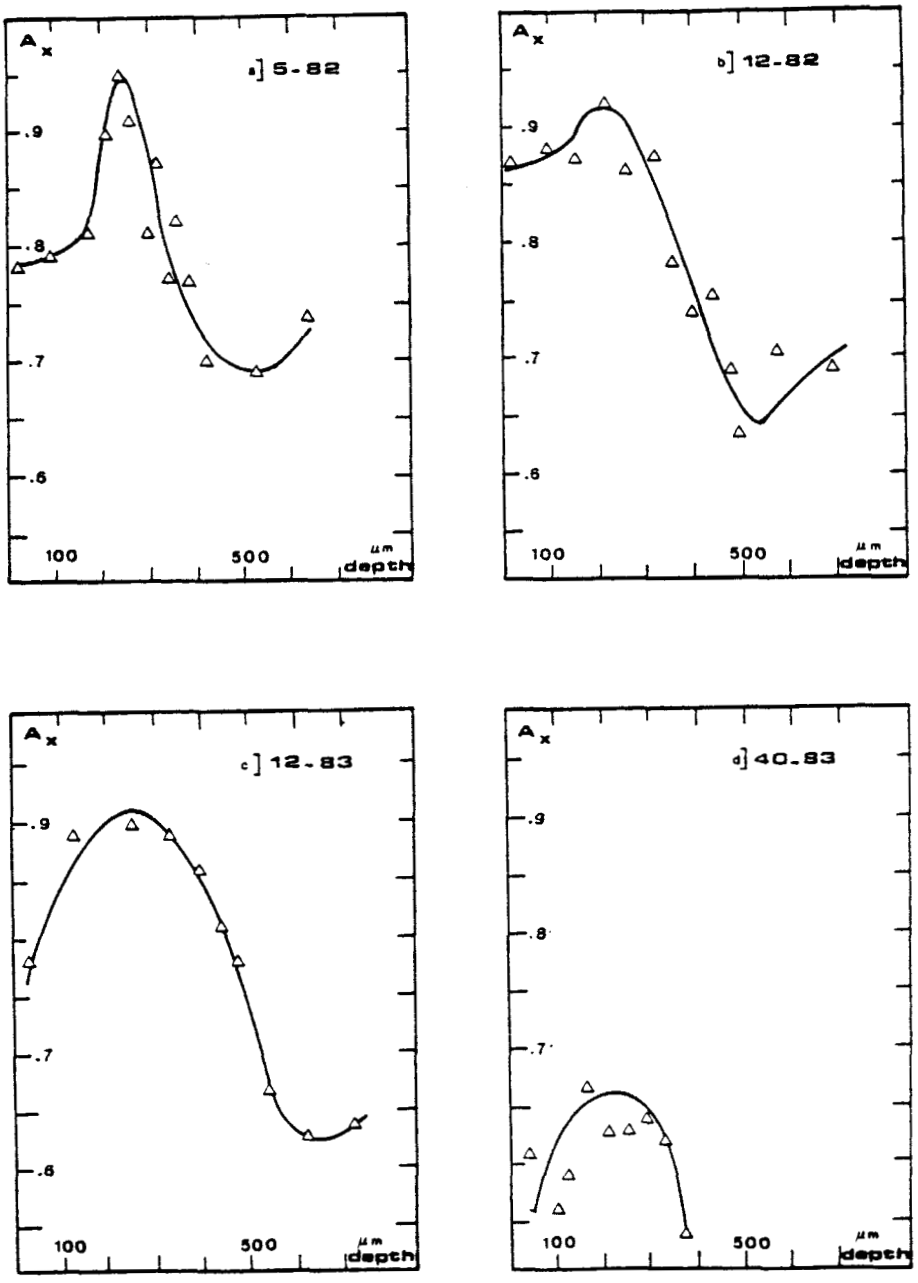

Fig. 7. Depth distribution of the crystalline orientation factor A from WAXS measurements for the 1G5 section: (a) PP/5/82; (b) PP/12/82; (c) PP/12/83; (d) PP/40/83.

lower for PP/40. This can be explained by the low molecular weight of the latter, which results in a low viscosity, e.g., in a low intensity of shear stresses, and in a high rate of orientation relaxation at a given temperature.

- For section 5, the orientation maximum is located at a depth (220–250 μm) practically constant, which was not the case for X_c. In the case of section 3 of PP 12/83, a noticeable shift towards the surface can be observed [Fig. 9(b)].

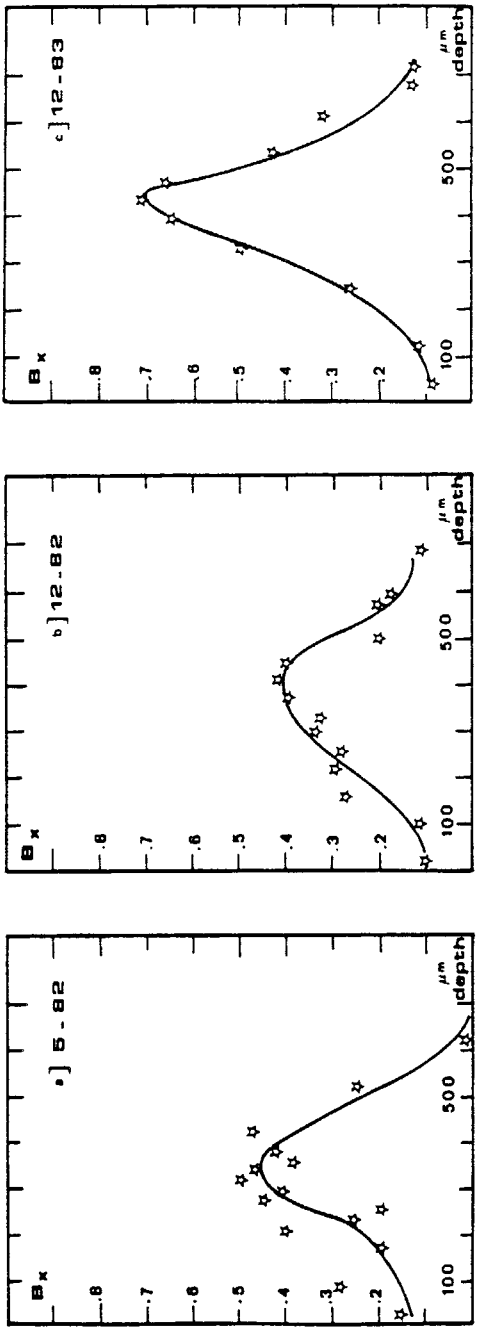

Fig. 8. Depth distribution of the beta fraction index B from WAXS measurements for the 1G5 section: (a) PP/5/82; (b) PP/12/82; (c) PP/12/83.

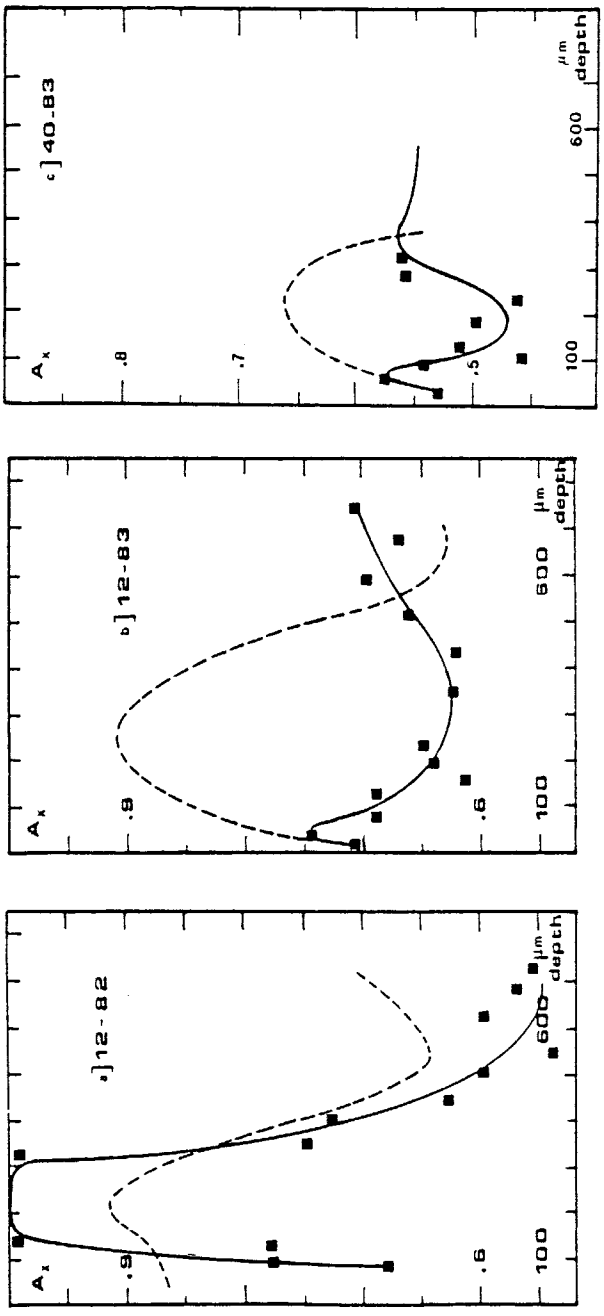

Fig. 9. Depth distribution of the crystalline orientation factor A for the 1G3 section: (a) PP/12/82; (b) PP/12/83; (c) PP/40/83; (---) distribution for section 5; (■) distribution for section 3.

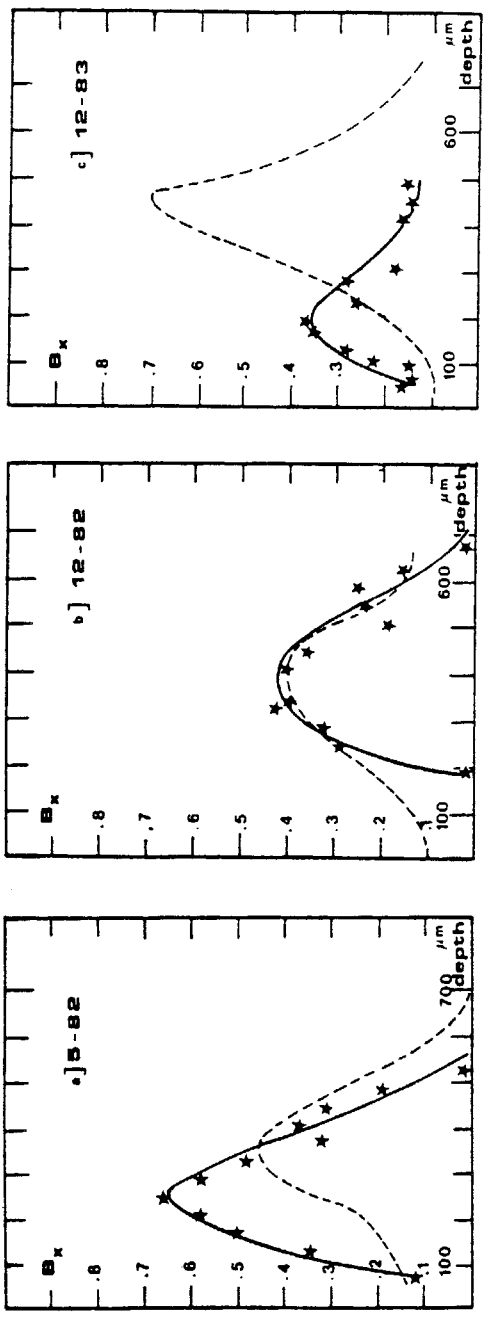

Fig. 10. Depth distribution of the beta fraction index B for the 1G3 section: (a) PP/5/82; (b) PP/12/82; (c) PP/12/83; (---) distribution for section 5; (★) distribution for section 3.

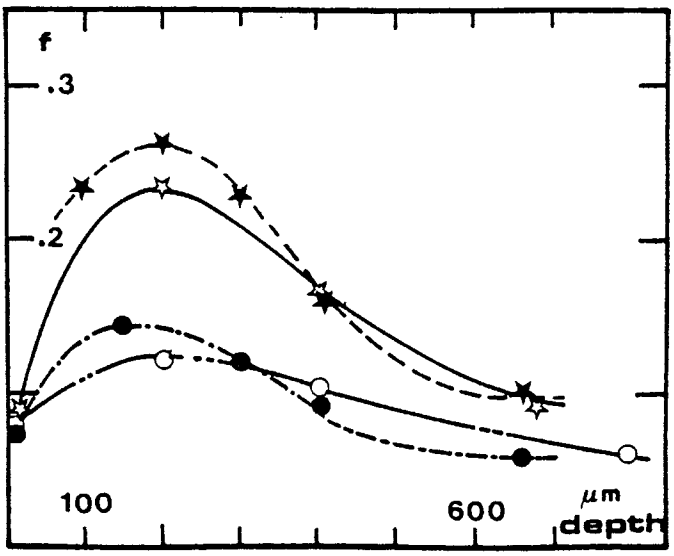

Fig. 11. Depth distribution of the crystalline (f_c) and amorphous (f_{am}) orientation factors from IR measurements for PP 12/82 in sections 5 and 3: (★) f_c for 1G3; (☆) f_c for 1G5; (●) f_{am} for 1G3; (○) f_{am} for 1G5.

- The beta phase is only found in a relatively sharp range of 200–500 μm thickness, centered in zone III of the PP/5 and PP/12 samples (no beta phase is found in PP/40). It should be remembered that the conditions for nucleation and growth of beta crystallites are: a macromolecular orientation in the melt, quick cooling down to 100–125°C, e.g., below the range of maximum rate of crystallization for the alpha form, and a high pressure.[11] The orientation condition can explain, at least partially, the complete lack of beta phase in PP/40, and the shift towards the surface of the B distribution curve for section 3 of PP 12/83 relative to section 5 [Fig. 10(c)].

Infrared Dichroism

In all cases, the IR dichroïsm data agrees with the WAXS data: the orientation maximum is located in the subskin region. The distributions of crystalline (f_c) and amorphous (f_{am}) orientation factors are presented, only for PP 12/82, in Figure 11.

In the calibrated part of the PP 12/82 tensile bar; the maximum of the f_c or f_{am} distribution curve is deeper (Fig. 12), and its intensity lower (Fig. 13), as the distance from the injection gate is greater. Similar observations were made by Kamal and Moy[7] in the case of polyethylene.

DISCUSSION

The above results might be explained by the combination of as few as two factors: the depth distribution of cooling rates, and the melt orientation in the shear zone, the latter favoring the local crystallization and nucleation of beta crystallites. According to this hypothesis, the depth distribution of X, A, B, f_c and f_{am} would be more or less superposable and would coïncide with the microscopic observations for a given sample. A detailed observation shows clearly that this is not the case, the depth of the maxima are generally in the

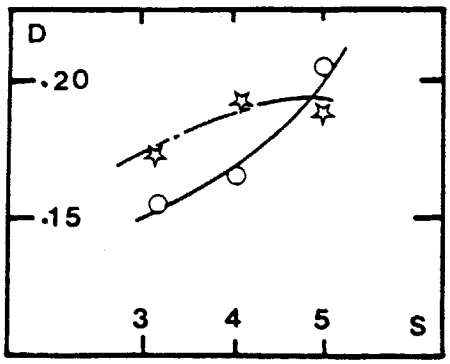

Fig. 12. Longitudinal distribution of the depth (D) of the maximum of f_c and f_{am} in PP 12/82: (☆) depth of f_c; (○) depth of f_{am}.

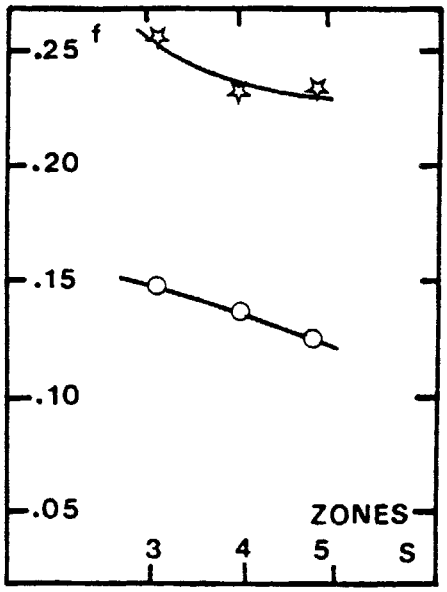

Fig. 13. Longitudinal intensity distribution of f_c (☆) and f_{am} (○) maximum for PP 12/82.

following order: bright zone II in micrographs = 100–230 μm; A = 220–250 μm; B = 300–425 μm.

We first tried to explain these results by the self-heating due to the high shear stresses which can locally reduce the quenching effect[16]; however, this hypothesis is not consistent with the presence of a minimum of X_c in high orientation zones, for instance, in the case of PP 12/82.

The noticeable differences existing between PP 12/82 and PP 12/83 seem to reveal a great effect of the holding pressure: the secondary maximum of crystallinity X_c is considerably shifted towards the core: 230 μm in 83 against 100 μm in 82, when the holding phase is delayed and the holding pressure lowered (Fig. 3).

An explanation of the above results can be proposed on the basis of the two following sets of data:

- Local cooling rates and temperatures of crystallization

It can be supposed from DSC experiments and literature data, that during cooling, crystallization begins at an appreciable rate at T_c = 130–150°C. To estimate the rate of penetration of the isotherm towards the core, we can use the data on PP cooling kinetics of Fitchmun and Mencik[3] since the experimental conditions are almost similar. Thus, it can be assumed that the front of crystallization penetrates the sample at 100–200 μm/s during the first seconds of cooling in the mold.

- Influence of pressure on crystallization

We must consider the influence of a pressure of 50–100 MPa on the crystallization kinetics in nonisothermal conditions. Since the crystallization temperature range is always contained between T_g (glass transition temperature) and T_m (melting point), it seemed to us interesting to appreciate the effect of the pressure on these transition temperatures.

The change of T_g can be estimated from the first law of Ehrenfest:

$$\frac{dT_g}{dP} = \frac{T_g \cdot V_g \cdot \Delta\alpha}{\Delta C_p}$$

where V_g is the molar volume at T_g: $V_g \simeq 50 \times 10^{-6}$ m^3/mol. $\Delta\alpha$ and ΔC_p are respectively the differences of expansivity and heat capacity between the liquid and glassy state.

The Simha–Boyer rule[17] gives $\Delta\alpha T_g = 0.115$; and Van Krevelen[18] ΔC_p = 225 mol^{-1} K^{-1}. Then

$$\frac{dT_g}{dP} \simeq 2.6 \times 10^{-7} \text{ K Pa}^{-1}$$

That leads for a holding pressure of 75 MPa to $\Delta T_g \simeq 20$°C.

The change of T_m can be estimated from the experimental results of Reinshagen and Dunlap[19]: $\Delta T_m/\Delta P \simeq 4.5 \times 10^{-7}$ K Pa^{-1} e.g., ΔT_g = 34°C for ΔP = 75 MPa.

It is therefore physically reasonable to suppose that the curve of crystallization rate versus temperature is shifted by 20–30°C towards the high temperatures when the holding pressure increased (Fig. 14).

Thus, in molding conditions, where the temperature decreases continuously, if the sample undergoes a sudden increase of pressure at time t, the crystallization rate will decrease in the layer where, at this time, $T = T_c$, and increase suddenly in an inner layer where, at this time, $T_p = T_c + 20/30$°C. The intermediary layer which will never reach its maximum temperature of crystallization rate T_{p_1}, and, even if it is well oriented, it will be characterized by a low degree of crystallinity. Indeed, the localization of the corresponding morphological "perturbation" will be all the sharper as the pressure increase (50 MPa s^{-1} in our case), and the local cooling (10°C s^{-1} in the subskin region) is faster. In other words the sudden increase of pressure, at the beginning of the packing, can be considered as a quenching in the layer limited, at the same, by the isotherms t_c and t_p.

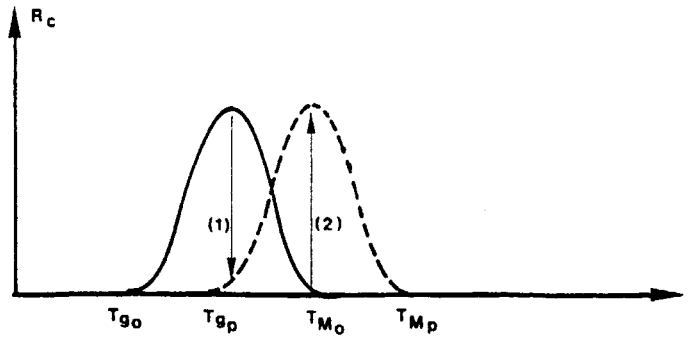

Fig. 14. Diagrammatic representation of the pressure effect on the crystallization rates: (0) ambient pressure; (p) under holding pressure. The arrows indicate the changes of crystallization rate occurring when the holding pressure is applied: (1) at isotherm T_c; (2) at isotherm $T_c + 30\Delta T_c$ (see text).

Now, the molding process can be decomposed into four elementary steps:

1. Mold Filling Step [Fig. 15(a)]. During this first step, the melt temperature is above the crystallization range, except in the immediate vicinity of mold walls where the amorphous skin is quickly solidified. The shear stresses, whose intensity, linked to the injection rate, is higher in conditions 82 than in 83 ones, are responsible for the subskin macromolecular orientation which is probably maximum at a depth higher than 250 μm. The pressure is low.

2. Prepacking Step. When the mold is filled, the flow is stopped, but the pressure remains low for a fraction of second. The orientation begins to relax in the inner layers but is frozen in the outer ones which are quickly cooled. When the subskin temperature reaches 150°C, the crystallization begins, probably at relatively high rate because it is favored by the macromolecular orientation. The form α predominates over the form β owing to the low pressure.

3. Onset of the Packing Stage [Fig. 15(b)]. After almost 2 s, the pressure increases suddenly. The front of crystallization, which is located at a distance d from the surface, jumps by Δd towards the core. According to Fitchmun and Mencik,[3] d = 100–200 μm for t = 2 s and $\Delta d \geq 100$ μm for $\Delta T_c \geq 20$°C. As expected, a zone of decreasing crystallinity is found between 100–200 and 500 μm. The longer the phase is delayed, the deeper the zone becomes, and the X_c decay is as sharper as the perturbation occurs near the surface, e.g., the local cooling rate is higher [compare the X_c profiles for PP 12/82 and PP 12/83 in Fig. 6(b)–(c)].

A second pressure effect concerns the orientation depth distribution. Since the pressure results in a free volume reduction, e.g., in a decrease of the macromolecular mobility, the rate of orientation relaxation is considerably reduced. This "pressure quenching effect" is especially noticeable in section 3 of PP 12/82 and PP 12/83 [Figs. 9(b) and (c)]. Indeed, since the cooling rate is the lower, the shorter is the distance to injection gate, the orientation relaxation in inner layers is more efficient in section 3 than in section 5, which explains the shape of the curves in Figure 12 whereas the decrease of orientation along flow axis (Fig. 13), which was previously studied,[10] can be explained by simple fluid mechanics considerations.

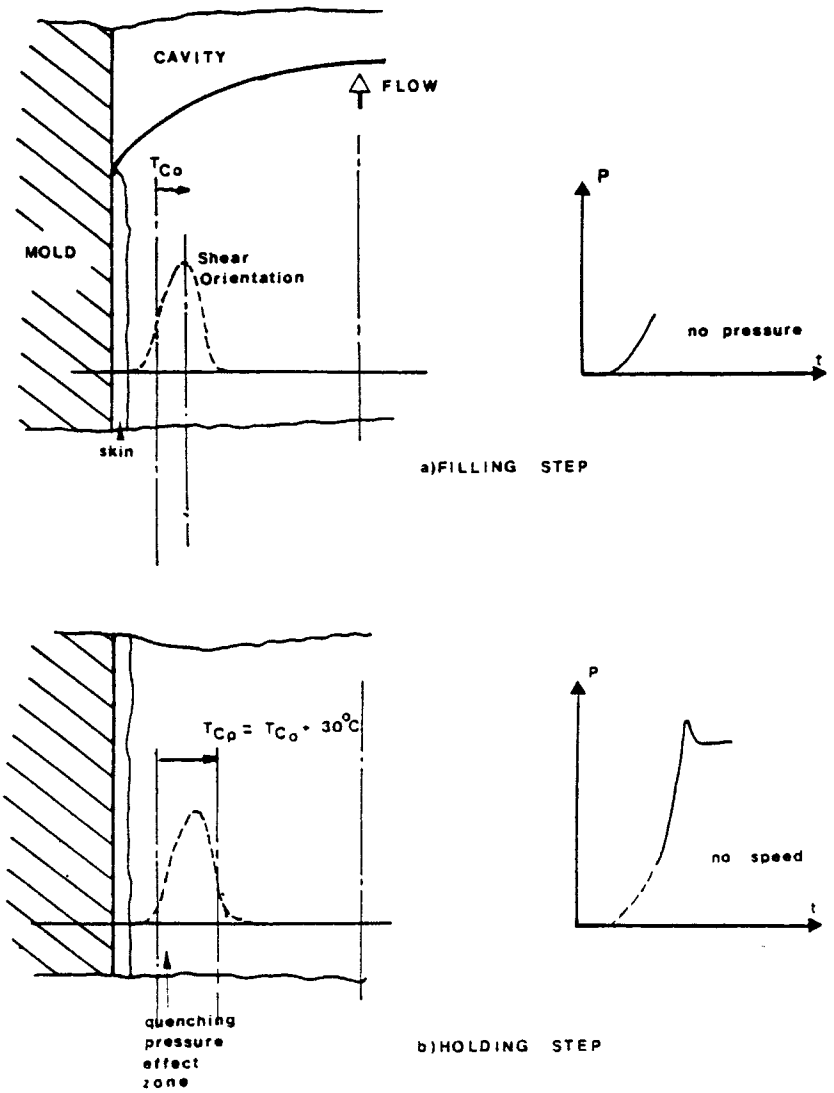

Fig. 15. Schematic sketch of the displacement of T_c when the pressure is set up in the mold.

A third pressure effect concerns the beta phase distribution: The high pressure and a quenching effect allow the nucleation and growth of beta crystallites, but only where the macromolecules are oriented. It is therefore not surprising to find the B distribution curves shifted towards the core relative to the X_c ones. The lack of beta crystallites in PP/40 has been explained in the section "results."

4. End of the Molding Cycle. Once the front of crystallization has passed through the oriented layer, e.g., for a depth higher than 500 μm, the nucleation of alpha crystallites becomes largely predominant. The low cooling rate allows a spherulitic growth. The well-known influences of cooling rate, molecular weight, and pressure on the degree of crystallinity or the sperulite diameter can be observed.

CONCLUSION

The above results reveal a complex morphological stratification in injection molded pieces of PP. The depth distribution of the crystalline ratio, macromolecular orientation, and beta phase fraction in the crystalline phase can be explained by the effects of cooling kinetics, injection rate, and holding pressure. The latter parameter plays a key role in the buildup of the morphology in the subskin region (100–500 μm depth), whose importance in fatigue behavior will be shown in the Part II of this paper.

References

1. M. R. Kantz, H. D. Newman Jr., and F. H. Stigale, *J. Appl. Polym. Sci.*, **16**, 1249 (1972).
2. M. R. Kantz, *Int. J. Polym. Mater.*, **3**, 245 (1974).
3. D. R. Fitchmun and Z. Mencik, *J. Polym. Sci.*, **11**, 951 (1973).
4. D. E. Scherpereel, *Plast. Eng.* **47** (Dec.), (1973).
5. M. Fujiyama, H. Awaya, and Z. Kimura, *J. Appl. Polym. Sci.* **21**, 3291 (1977).
6. M. Fujiyama and K. Azuma, *J. Appl. Polym. Sci.*, **23**, 2807 (1979).
7. M. R. Kamal and F. H. Moy, *J. Appl. Polym. Sci.*, **28**, 1787 (1983).
8. J. P. Trotignon and J. Verdu, *Interrelationships between Processed Structures and Properties of Polymer Materials*, Seferis, Ed., Elsevier, New York, 1984, p. 471.
9. A. T. Lovinger, J. O. Chua, and C. C. Gyrpte, *J. Polym. Sci.*, **15**, 641 (1977).
10. J. P. Trotignon, J. L. Lebrun, and J. Verdu, *Plast. Rubber Process. Appl.*, **2** (3), 247 (1982).
11. A. Turner-Jones, J. M. Aizelewood, and D. R. Beckett, *Makromol. Chem.*, **75**, 134 (1964).
12. R. J. Samuels, *Structured Polymer Properties*, Wiley, New York, 1974.
13. B. Wunderlich, in *Macromolecular Physics*, Academic, New York, 1976, Vol. 2.
14. J. Bowman, N. Harris, and M. Bevis, *J. Mater. Sci.*, **10**, 63 (1975).
15. Z. Tadmor, *J. Appl. Polym. Sci.*, **18**, 1753 (1974).
16. L. Schmidt, J. Opfermann, and G. Menges, *Polym. Eng. Rev.*, **1** (1), 1 (1981).
17. R. Simha and R. F. Boyer, *J. Chem. Phys.*, **37**, 1003 (1962).
18. Van Krevelen, in *Macromolecular Physics*, Academic, New York, 1976, Vol. 2.
19. J. H. Reinshalen and R. W. Dunlap, *J. Appl. Polym. Sci.*, **20**, 9 (1976).

Received March 14, 1986
Accepted July 10, 1986